PROCEEDINGS A

rspa.royalsocietypublishing.org

Research

Cite this article: Moulton DE, Lessinnes T, O'Keeffe S, Dorfmann L, Goriely A. 2016 The elastic secrets of the chameleon tongue. *Proc. R. Soc. A* **472**: 20160030.
http://dx.doi.org/10.1098/rspa.2016.0030

Received: 13 January 2016
Accepted: 16 March 2016

Subject Areas:
biomechanics, mathematical modelling

Keywords:
nonlinear elasticity, active forces, ballistic motion, energy conversion

Author for correspondence:
Derek E. Moulton
e-mail: moulton@maths.ox.ac.uk

The elastic secrets of the chameleon tongue

Derek E. Moulton[1], Thomas Lessinnes[1], Stephen O'Keeffe[1], Luis Dorfmann[2] and Alain Goriely[1]

[1]Mathematical Institute, University of Oxford, Oxford, UK
[2]School of Engineering, Tufts University, Medford, MA, USA

AG, 0000-0002-6436-8483

The ballistic projection of the chameleon tongue is an extreme example of quick energy release in the animal kingdom. It relies on a complicated physiological structure and an elaborate balance between tissue elasticity, collagen fibre anisotropy, active muscular contraction, stress release and geometry. A general biophysical model for the dynamics of the chameleon tongue based on large deformation elasticity is proposed. The model involves three distinct coupled subsystems: the energetics of the intralingual sheaths, the mechanics of the activating accelerator muscle and the dynamics of tongue extension. Together, these three systems elucidate the key physical principles of prey-catching among chameleonides.

1. Introduction

Among animals, chameleons have strikingly distinctive features: they have zygodactylous feet, prehensile tails, colour-changing ability, panoramic eyes and ballistic projection of their tongue for prey-catching. What distinguishes prey-catching in chameleons is not only the extension of the tongue—up to 2.5 body lengths—but also the extreme acceleration and short duration of the entire ballistic projection (figure 1). Anderson [1] estimates the total duration of tongue projection, depending on species, to last between 10 and 55 ms. Maximum accelerations between 500 and 2590 $\mathrm{m\,s^{-2}}$ are reported, requiring peak power density between 3000 and 14 040 $\mathrm{W\,kg^{-1}}$ [1–4]. The accepted theory is that the tongue projection is triggered entirely by intrinsic muscular activities [5]. It is further understood that the peak power recorded in tongue extension cannot be solely due to muscle activation, but is the result of a release of the energy stored in the extension of the

THE ROYAL SOCIETY PUBLISHING

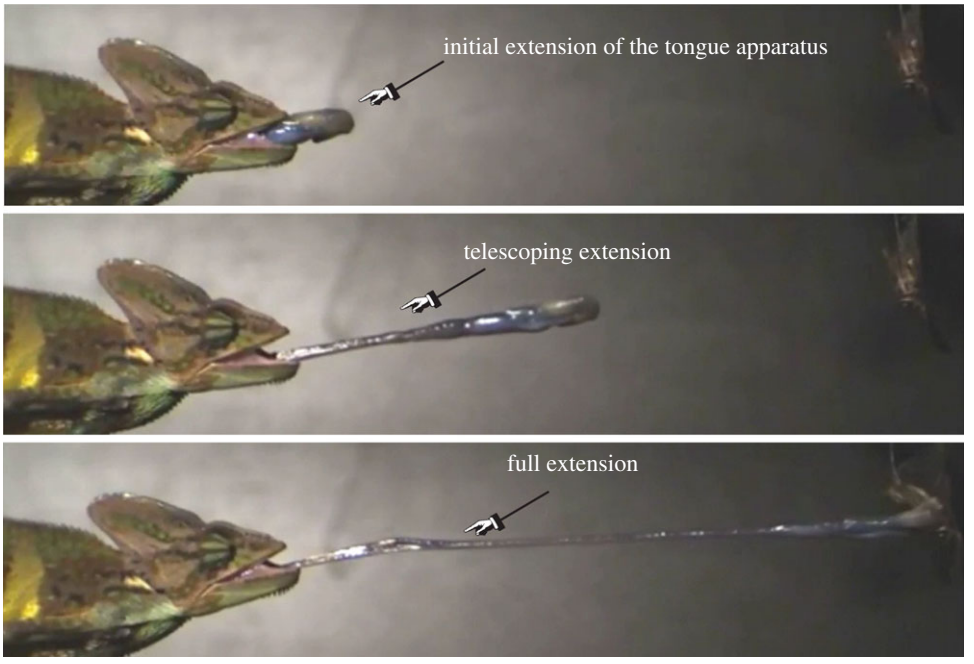

Figure 1. Tongue ejection in *Chamaeleo calyptratus*. Images courtesy of Stephen Deban. (Online version in colour.)

tongue's collagenous tissue [3]. By contrast, the relatively slow process of tongue retraction results from direct muscular contraction as demonstrated experimentally [6]. The chameleon's ballistic mechanism is a clear example in biology of elastic forces generating rapid motion [7]. This remarkable process has been studied since the seventeenth century [8–10] and has received considerable interest in recent decades, primarily in experimental biology [3,6,11–13], but also from theoretical [14] as well as biomimetic [15] perspectives. Tongue projection and prey-catching in salamanders, which rely on a different mechanism, has also been extensively investigated [16,17]. Despite such interest, a complete biomechanical model describing the storage and release of energy in the chameleon tongue is lacking. The purpose of this paper is to provide such a model, to explain the key features and advantages of this system, and to examine the mechanism from an engineering design perspective. From a theoretical point of view, the modelling of such a phenomenon is also particularly interesting as it naturally combines large deformation solid mechanics together with the modelling of anisotropic response and active muscular contraction. These features appear in many diverse biomechanical systems such as arteries, elephant trunks, stems and in the rapid release of seeds [18–21].

There are three main processes of interest related to the tongue projection: (i) the muscle fibres in the accelerator muscle are activated and produce mechanical work, (ii) elastic energy is stored in tubular-shaped collagenous intralingual sheaths, and (iii) the stored energy is rapidly released and converted into kinetic energy to generate ballistic projection [22,23]. The tongue of the chameleon rests on a rigid bone-like structure, the entoglossal process (called here *the bone*). The tongue complex itself is made of connected tubular units: the intralingual sheaths and the accelerator muscle (figure 2). For reference, we place a cylindrical coordinate system along the axis of the tongue, taken as the z-axis. The intralingual sheaths are almost exclusively made of collagen [3,24] with collagen fibrils organized in pairs of equal and opposite helical fibres along the z-direction, preventing torsional shear while providing extensibility. On the bone, the intralingual sheaths are concentrically stacked (figure 2), so that it appears mechanically as n thin tubular cylinders. As the tongue is ejected, the sheaths extend telescopically, (not unlike the popular laser saber toy from the Star Wars franchise), until fully extended (figure 1). Surrounding

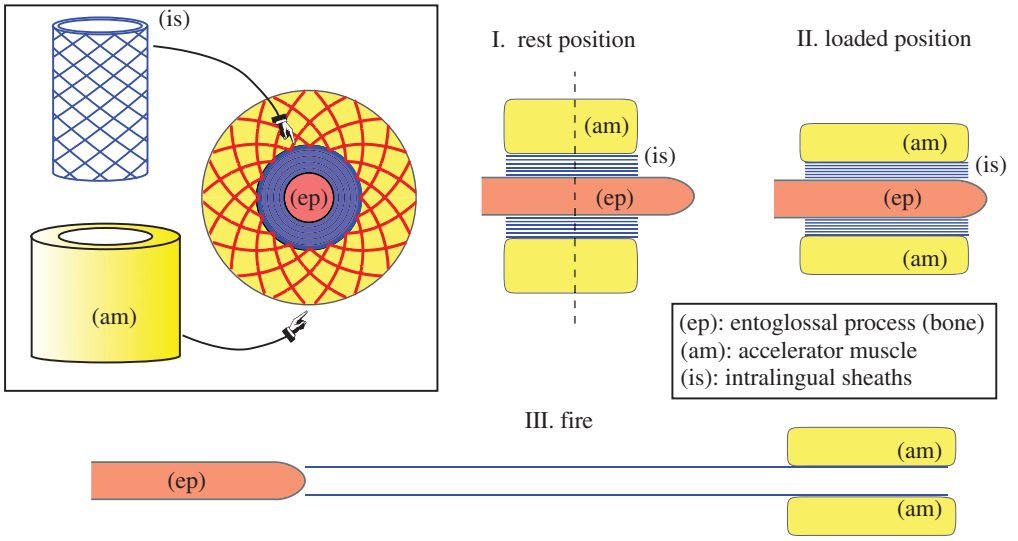

Figure 2. Inset: cross section of the tongue complex composed of the entoglossal process (bone), intralingual sheaths (with collagen fibres) and accelerator muscle (with helical muscular fibres). The complex has three key positions: I. The rest position in the absence of muscular activity, II. The extended loaded position after muscular activity, and III. The fire position when the tongue slips off the bone. (Online version in colour.)

the sheaths is the accelerator muscle, a thick tubular unit attached to the outermost intralingual sheath and ejected during ballistic projection. The muscle fibres in this unit are oriented in a plane perpendicular to the axis. Before muscular activation, the system is *at rest* on the bone. As the muscle fibres contract, the accelerator muscle squeezes the intralingual sheaths and extends them closer to the tip, the *loaded position*. From that position, a further small contraction will allow the entire complex to *fire* by sliding off the tapered tip, quickly converting its elastic potential energy into kinetic energy. The tongue structure and positions are shown schematically in figure 2. We first develop a biomechanical description of this structure in §2 within the theory of nonlinear elasticity by modelling the tongue tissues as elastic fibre-reinforced tubular units under the action of muscular contraction. To elucidate the roles of the muscle and the sheaths and the effect of geometry on the mechanism, in §3, we compare the energy, stresses and deformations generated in the system in the rest and loaded positions. To explore the physics involved in the energy release, in §4, we use the force applied on the bone and the elasticity of the system to model the dynamics of the firing.

2. Model development

(a) Set-up

As depicted in figure 3, we model the bone as a cylinder of radius ρ with a tapered end and the tongue complex as $n+1$ hyperelastic cylindrical shells composed of n *intralingual sheaths* of unstressed lengths L_i, inner radii A_i, and outer radii $B_i = A_i + h$, for $i = 1, \ldots, n$; and the *accelerator muscle* with unstressed length L_{n+1} and inner and outer radii A_{n+1}, B_{n+1}, respectively. The material is assumed incompressible both for convenience in finding analytical solutions, and owing to the fact that most collagenous soft tissues are nearly incompressible. We assume, in this analysis, that each tube remains cylindrical while on the bone. Let a_i and b_i be the inner and outer radii, respectively, of the ith tube in the rest position and $\tilde{a}_i$ and $\tilde{b}_i$ the corresponding values in the loaded position, such that $a_1 = \tilde{a}_1 = \rho$.

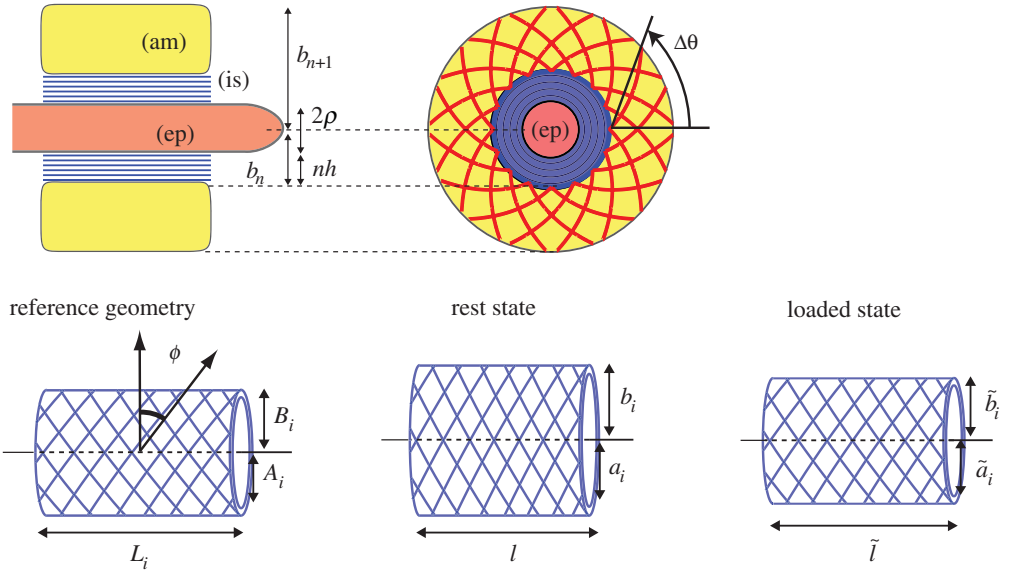

Figure 3. Geometry of the tongue complex and intralingual sheaths. The bone (ep for entoglossal process), with radius ρ, is surrounded by n concentric intralingual sheaths (is) and the accelerator muscle (am). The accelerator muscle contains embedded fibres arranged in a logarithmic spiral characterized by angle $\Delta\theta$. On the bone, the inner radius of the first sheath is $a_1 = \rho$. Off the bone, the reference radius is $A_1 \leq \rho$ with reference fibre angle ϕ. (Online version in colour.)

Both the sheaths and the accelerator muscle contain embedded fibres. The sheaths are reinforced by collagen fibrils arranged in pairs of oppositely oriented helices. We let ϕ denote the angle the fibres make with the circumferential direction in the reference geometry (figure 3). The accelerator muscle contains cross-sectional fibres arranged in logarithmic spirals [22], the tightness of which is characterized by angle $\Delta\theta$ (figure 3). The firing mechanism is activated by contraction of these fibres, which is accounted for by a parameter ν appearing in the energy [25], such that $\nu = 1$ at rest and $\nu < 1$ in contraction.

We assume that both sheaths and muscle remain connected, so that the outer radius of the ith tube equals the inner radius of the $(i+1)$th tube for $i = 1, \ldots, n$, and all tubes have length l at rest and length $\tilde{l}$ when loaded. The accelerator muscle is assumed to be stress free in the rest position ($A_{n+1} = b_n$) but we allow for the possibility that the sheaths are radially stretched in this position, so that $0 < A_i \leq a_i$ for $i = 1, \ldots, n$. We use the standard cylindrical coordinates (R, Θ, Z) to denote a material point in the reference configuration and (r, θ, z) to denote the same point in a deformed configuration, both in the basis $(\mathbf{e}_r, \mathbf{e}_\theta, \mathbf{e}_z)$.

(b) Mechanical equilibrium

The elastic strain–energy in the system is given by the sum of the energy density W_{is} of the intralingual sheaths (which depends on their reference radii A_i and the fibre angle ϕ) and the energy density W_{am} of the accelerator muscle (depending on the contraction ν of the muscle fibres):

$$\mathcal{E} = 2\pi\zeta l \left[\int_{\rho}^{b_n} W_{\mathrm{is}}(r, \zeta; A_i, \phi) r \, \mathrm{d}r + \int_{b_n}^{b_{n+1}} W_{\mathrm{am}}(r, \zeta; \nu) r \, \mathrm{d}r \right],$$

where $\zeta = \tilde{l}/l$ is the axial extension ($\zeta = 1$ in the rest position, $\zeta > 1$ in the loaded position).

For given reference parameters and for a given contraction ν, the problem is to obtain the extension ζ by minimizing this energy. Once the extension is known, we compute the energy in the loaded position. To solve this problem, we write the elastostatic boundary-value problem

associated with the minimization of this energy. That is, we balance the forces with the condition of no axial loading on the faces, a stress-free boundary on the outer cylinder, and a fixed radius on the inner cylinder, corresponding to the fixed bone radius ρ. This approach also provides the pressure of the tongue complex on the bone, which will play a key role in the tongue dynamics.

The deformation of each tube is determined as follows. In the absence of torsion, each tube can inflate and extend, so that its deformation is simply given by

$$r = r(R), \quad \Theta = \theta \quad \text{and} \quad z = \zeta Z, \tag{2.1}$$

where ζ is the constant axial stretch and $r(R)$ a function to be determined. It is standard to show [26] that the deformation gradient is

$$\mathbf{F} = r'(R)\mathbf{e}_r \otimes \mathbf{e}_r + \frac{r}{R}\mathbf{e}_\theta \otimes \mathbf{e}_\theta + \zeta \mathbf{e}_z \otimes \mathbf{e}_z, \tag{2.2}$$

where $\otimes$ denotes the standard tensorial product. We can use the incompressibility condition $\det \mathbf{F} = r' r \zeta / R = 1$ to obtain an explicit form for the deformation:

$$r = \sqrt{a^2 + \frac{R^2 - A^2}{\zeta}}. \tag{2.3}$$

The outer radius in the current configuration is then given by

$$b = \sqrt{a^2 + \frac{B^2 - A^2}{\zeta}}. \tag{2.4}$$

Because the deformation is diagonal in cylindrical coordinates and only depends on R, the Cauchy stress tensor, $\mathbf{T}$, is also diagonal in these coordinates, so that

$$\mathbf{T} \equiv \mathrm{diag}(t_r, t_\theta, t_z) \equiv t_r \mathbf{e}_r \otimes \mathbf{e}_r + t_\theta \mathbf{e}_\theta \otimes \mathbf{e}_\theta + t_z \mathbf{e}_z \otimes \mathbf{e}_z. \tag{2.5}$$

This particular form of the Cauchy stress tensor implies that the Cauchy equation for the equilibrium of an elastic material in the absence of body forces, $\mathrm{div}\, \mathbf{T} = \mathbf{0}$, in cylindrical coordinates reduces to a single scalar equation

$$\frac{\mathrm{d}t_r}{\mathrm{d}r} + \frac{1}{r}(t_r - t_\theta) = 0. \tag{2.6}$$

Equation (2.6) can be integrated over r with the proper boundary condition

$$t_r(b) - t_r(a) = \int_a^b \frac{t_\theta - t_r}{r}\, \mathrm{d}r. \tag{2.7}$$

To obtain stresses and strains, we need to specify a strain–energy density function that gives the energy stored in a particular deformation. The sheaths are modelled by the standard fibre-reinforced strain–energy density function [27]. The idea is to penalize the energy in deformations along the directions $\mathbf{M}_\pm$ of fibres modelled as a continuous field. That is, in addition to the classic quadratic form of the energy in terms of the strains, we add a contribution owing to the fibres, so that we have now:

$$W_{\mathrm{is}} = \mu_{\mathrm{is}}[(I_1 - 3) + \alpha_{\mathrm{is}}((I_+ - 1)^2 + (I_- - 1)^2)] \tag{2.8}$$

with

$$I_1 = \mathrm{tr}(\mathbf{C}) \quad \text{and} \quad I_\pm = \mathbf{M}_\pm \cdot (\mathbf{C}\mathbf{M}_\pm). \tag{2.9}$$

and $\mathbf{C} = \mathbf{F}^{\mathrm{T}}\mathbf{F}$ is the right Cauchy–Green stretch tensor that contains all information regarding stretches. The invariants $I_\pm$ express the stretch in the direction of the fibres. Note that this particular form of stretch is written in a way such that in all deformations, the invariants express the fibre stretch even if the fibre orientation changes. Here,

$$\mathbf{M}_\pm = \cos\phi\, \mathbf{e}_\theta \pm \sin\phi\, \mathbf{e}_z \tag{2.10}$$

denotes the orientation of the fibres taken to be tangent to the cylinder at each point (figure 3).

The accelerator muscle is also described by a fibre-reinforced strain-energy density function modified to take into account the muscular contraction:

$$W_{\mathrm{am}} = \mu_{\mathrm{am}}[(I_1 - 3) + \alpha_{\mathrm{am}}((I_+ - \nu)^2 + (I_- - \nu)^2)], \tag{2.11}$$

with

$$I_1 = \mathrm{tr}(\mathbf{C}) \quad \text{and} \quad I_\pm = \mathbf{N}_\pm \cdot (\mathbf{C}\mathbf{N}_\pm). \tag{2.12}$$

The muscle fibres are not organized into helices but in spirals (figure 3), so that

$$\mathbf{N}_\pm = \frac{\mathbf{e}_r \pm RG'\mathbf{e}_\theta}{\sqrt{(RG')^2 + 1}}, \quad \text{where} \quad G(R) = \frac{\Delta\Theta \log(R/A_{n+1})}{\log(A_{n+2}/A_{n+1})}, \tag{2.13}$$

corresponds to equal and opposite fibres arranged in logarithmic spirals in the plane normal to the cylinder axis [28]. As stated, the parameter ν controls the muscular contraction where $0 < \nu < 1$ corresponds to contraction and $\nu > 1$ is an extension [25].

Having defined the strain–energy density function for sheaths and muscle, the constitutive relation between the Cauchy stress tensor and the strain is

$$\mathbf{T} = -p\mathbf{I} + 2[W_1\mathbf{C} + W_+\mathbf{m}_+ \otimes \mathbf{m}_+ + W_-\mathbf{m}_- \otimes \mathbf{m}_-], \tag{2.14}$$

where p is a hydrostatic pressure that maintains incompressibility and $W_i = \partial_{I_i} W$, for $i \in \{1, +, -\}$ and $\mathbf{m}_\pm = \mathbf{F}\mathbf{M}_\pm$ for the sheaths and $\mathbf{m}_\pm = \mathbf{F}\mathbf{N}_\pm$ for the accelerator muscle.

The above-mentioned relation forms the mechanical constitutive description for each individual tube. To construct the tongue complex and determine the equilibrium configuration, the n sheaths are arranged concentrically on the bone followed by the accelerator muscle, with continuity of deformation ($a_{i+1} = b_i$) and traction ($t_r(a_{i+1}) = t_r(b_i)$) imposed at each interface. We then integrate (2.6) over all layers, with piecewise defined functions for stress and strain. The pressure P exerted by the tongue complex on the bone and the force F in the axial direction are given by [25]

$$P = \int_{\tilde{a}_1}^{\tilde{b}_{n+1}} \frac{t_\theta - t_r}{r}\,\mathrm{d}r \quad \text{and} \quad F = 2\pi \int_{\tilde{a}_1}^{\tilde{b}_{n+1}} t_r r\,\mathrm{d}r. \tag{2.15}$$

The boundary conditions in both rest and loaded position are $a_1 = \tilde{a}_1 = \rho$, corresponding to the tongue complex sitting on the bone, and no axial force on the faces, i.e. $F = 0$. These two conditions, together with the incompressibility condition, $r'(R)r\zeta = R$, are sufficient to determine the deformation, fully specified by the length $\tilde{l}$. The rest position is obtained by setting the muscular contraction $\nu = 1$, and the loaded position corresponds to a value $0 < \nu < 1$.

(c) Parameters

The base parameters that we have used in this model are provided in table 1. The geometric parameters for the bone, sheaths and accelerator muscle are as reported in [3] for *Trioceros jacksonii*. In cases where a particular parameter was not specifically stated in [3], they were estimated from images in [3]. Mechanical parameters correspond to typical values of shear moduli for fibrous biological tissues, accounting for fibre density as estimated from images in [3].

3. Energy build-up and extension

The two main quantities of interest in the deformation of the tongue from the rest to the loaded positions are the axial extension $\zeta = \tilde{l}/l$ and the elastic energy $\mathcal{E}$. In order to fire successfully, the contracting muscle must generate sufficient axial extension for the tongue complex to reach the tip of the bone, while at the same time developing enough elastic energy to achieve high velocity when converted to kinetic energy.

Table 1. Parameter values.

parameter	description	value
ρ	bone radius	1.4 mm
n	number of sheaths	10
A_1	inner sheath ref radius	1.4 mm
h	sheath ref thickness	0.05 mm
A_i	ith sheath ref radius	$1.4 + (i - 1)h$ mm
L	tongue length in rest state	15 mm
l_i	ith sheath ref length	15 mm
ϕ	sheath fibres orientation angle	50°
A_{n+1}	muscle ref inner radius	1.9 mm
B_{n+1}	muscle ref outer radius	2.5 mm
$\Delta\Theta$	muscle fibre spiral parameter	80°
μ_{is}	sheath shear modulus	1 kPa
μ_{am}	muscle shear modulus	1 kPa
$\mu_{\mathrm{is}}\alpha_{\mathrm{is}}$	sheath fibre shear modulus	0.1 GPa
$\mu_{\mathrm{am}}\alpha_{\mathrm{am}}$	muscle fibre shear modulus	0.1 GPa

(a) Role of sheaths

To understand the role of the sheaths in the mechanism, we plot, in figure 4, the elastic energy and axial extension for varying muscle contraction ν for two cases: base parameter values as reported in table 1 for *T. jacksonii*, and the case of an equivalent volume of accelerator muscle but with no sheaths present. As the muscle contracts, if there are no sheaths present, the muscle simply extends axially, attaining large extension ($\zeta = 1.4$ at $\nu = 0.86$) but building almost no internal energy. With sheaths, the axial extension is reduced, but the energy in both muscle and sheaths is an order of magnitude higher.

This computation demonstrates that the sheaths are crucial for the build-up of energy and that, with sheaths present, comparable energy is built-up in both the sheaths and the accelerator muscle. Essentially, in the absence of sheath, there is no resistance to axial extension, so upon muscle contraction the equilibrium configuration consists of a large extension and little stored energy. The sheaths provide strong resistance to axial extension, owing to the presence of the helical fibres, hence the extension is reduced and large elastic energy is stored. The degree of resistance and consequently, the amount of extension and stored energy is strongly dependent on the sheath angle. We explore this relationship in the following sections.

(b) Role of geometry

Having established the importance of the sheaths, we seek to understand the role of geometric parameters on the energy-building capabilities. There are numerous possible configurations and changes in geometry that could in principle be analysed. Here, we focus on two fundamental physical components that govern the energy storage and projectile capabilities of the tongue. One is the degree of pre-stretch, owing to any difference between the stress-free radii of the sheaths, A_i, and their radii in the rest position, a_i. Second is the fibre anisotropy, characterized by the angle ϕ. Note that the number and thickness of sheaths is only of secondary importance, because the thickness of the cylinder of stacked sheaths is the primary effect that enters the computation. We consider four representative combinations of these effects:

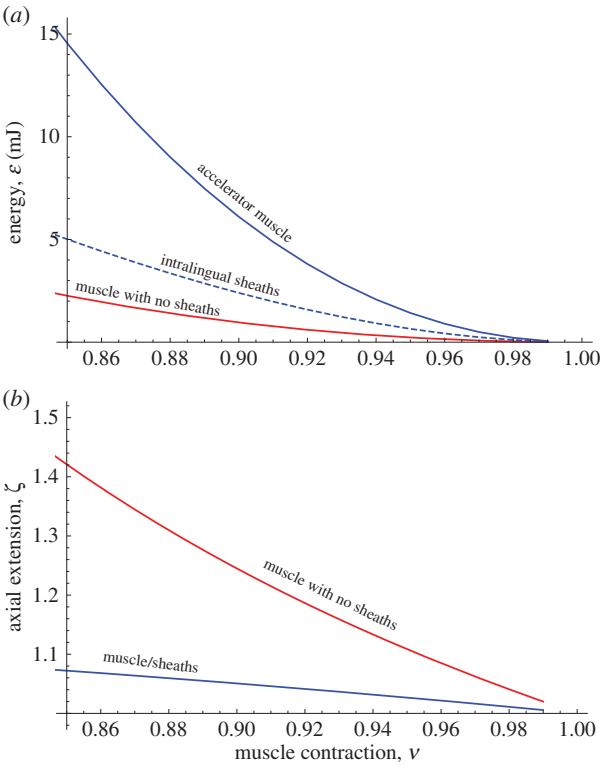

Figure 4. Elastic energy stored: without intralingual sheaths (red). In blue, the energy distributed in the sheaths (dashed) and in the muscles (solid) when both structures act together. (Online version in colour.)

— BASE: base values with stress-free sheaths: $A_i = a_i = \rho + (i-1)h$ for sheaths, $L_i = l$, and fibre angle $\phi = 50^\circ$, as used in figure 4;
— ANI: change of anisotropy by decreasing fibre angle to be less aligned with longitudinal axis: ϕ decreased from 50° to 30°;
— PRE: addition of pre-stress by decreasing sheath radii: $A_i = 1.35$ mm for all sheaths;
— ANI-PRE: decrease of both angle and radii, as above.

For consistent comparison, the total volume of sheaths, total mass of accelerator muscle and rest length l are taken to be equal for each case.

A schematic for these four cases is given in figure 5. In varying the A_i to incorporate pre-stress, our approach here is to take all sheaths to have the same reference radius, thus creating a substantial degree of residual stress (as opposed to taking $A_1 < \rho$ and $A_i = A_1 + (i-1)h$ for $i = 2, 3, \ldots n$). We note that not all parameter sets are even physically feasible, e.g. if we take $\phi = 30^\circ$ and $A_i = 1.35 + (i-1)h$, the rest state requires a negative pressure applied to the bone, i.e. the tongue would not sit on the bone in mechanical equilibrium without additional forces being imposed. We have chosen here a representative set of cases within the physically feasible range.

In figure 6, we plot the total stored energy and axial stretch as functions of the muscle contraction ν for the four cases. The comparison between the different cases leads to the following conclusions:

— comparing BASE and ANI demonstrates the significant effect of fibre angle. A decreased angle leads to a significant increase in axial extension but a large reduction in energy. For helical fibres more aligned with the circumferential direction, less resistance to extension is provided and less energy stored;

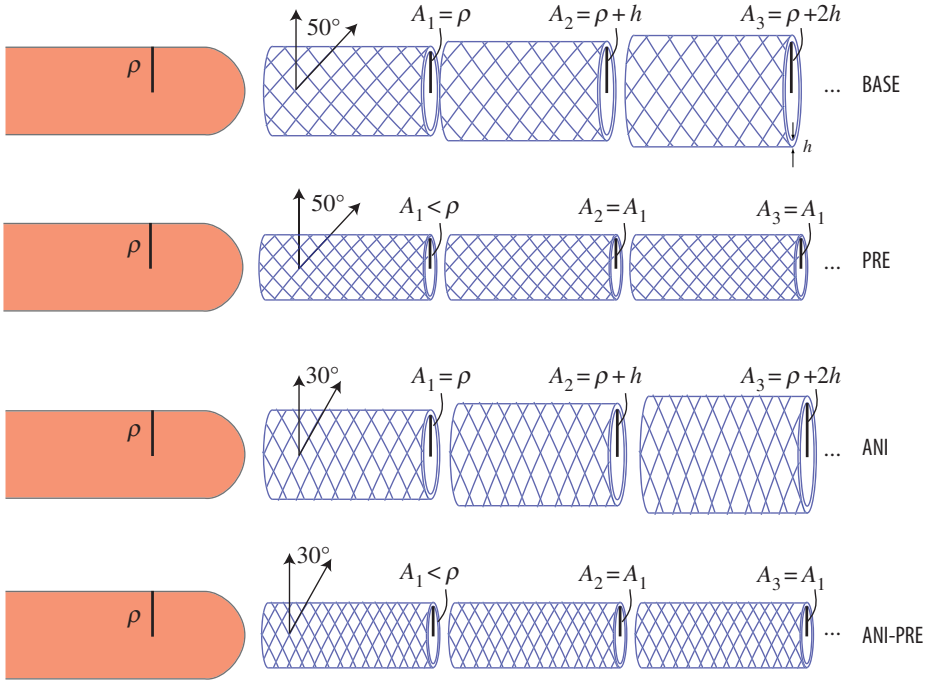

Figure 5. Schematic for the four different cases considered. (Online version in colour.)

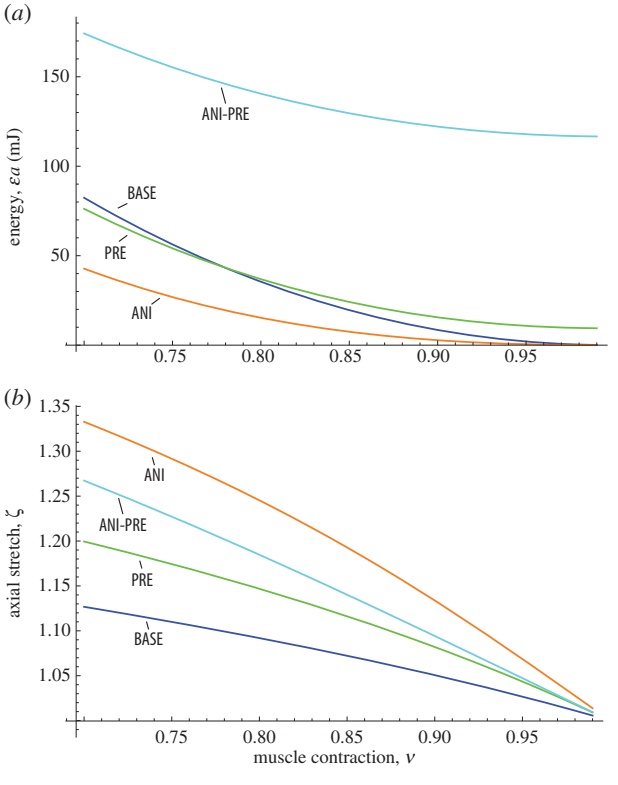

Figure 6. Elastic properties under different hypotheses as accelerator muscle contracts. (*a*) Total elastic energy and (*b*) axial extension. (Online version in colour.)

— comparing BASE and PRE shows improvement in axial extension with no significant changes in energy. The combination of pre-stress and anisotropy is more complicated owing to the highly nonlinear response of the structure; and
— looking at ANI-PRE, we see that the extension is increased (compared with PRE), but the total energy also increases, with more than double the amount at 30% contraction. However, in this case, the rest position ($\nu = 1$) has very high energy owing to the large residual stress. Hence, with pre-stress more work is needed to reload the apparatus on the bone after projection, and the structure would exert significant and potentially damaging force even at rest position. We conclude that while the benefit of extra axial extension and sensitivity to fibre angle may have interesting design implications for biomimetics [15], it is unlikely to be a key component in the chameleon's projection mechanism.

4. Energy release

The analysis of the stored elastic energy in the loaded position does not give us direct information on the dynamical process leading to prey catching. To catch its prey, this energy must be converted into kinetic energy in the axial direction, $K_z = mv_z^2/2$. The tongue complex for *T. jacksonii* weighs around 1 g and reaches a velocity of around 6 m s^{-1} [1,3,13], which requires 18 mJ of axial kinetic energy. Rapid motion is achieved when the tongue complex slides off the tapered tip of the bone, after which it is free to decrease the internal radius of the complex and reduce its internal elastic energy. Mechanically, the tongue complex acts equivalently to a series of connected springs pushed by a force in the axial direction. This force is the longitudinal component of the reaction force owing to the pressure exerted by the tongue at the tapered tip: the tapering acts as a launch pad for the release of the elastic energy.

(a) A model for dynamics

To simulate the dynamics and release of stored energy, we devise a map from the three-dimensional concentric tubes to a series of one-dimensional connected springs pushed by a force in the axial direction. In the loaded state, the tongue exerts a pressure on the bone, given by (2.15). Over the cylindrical portion of the bone, this pressure is balanced by a radial reaction force and the system is in mechanical equilibrium. However, in the tapered portion of the bone, the reaction force contains a longitudinal component, so that the tapered tip acts as a launch pad to convert the stored energy into kinetic energy. To model this process, we discretize the tongue complex along the z-direction and map the elastic properties of the $n+1$ layer cylinder to an effective spring constant and a one-dimensional force field provided by the full three-dimensional nonlinear model as shown in figure 7. For a given ν, the effective spring constant can be obtained from (2.15) as $K = \partial F/\partial\zeta$, evaluated at $\zeta(\nu)$.

To simulate the force applied to the tapered tip of the bone, we compute the pressure P_0 exerted by the tongue complex on the cylindrical portion of the bone, and the radius $\hat{\rho} < \rho$ at which no radial pressure is exerted. We computed the following values for the different cases: BASE: $\hat{\rho} = 1.01$ mm; ANI: $\hat{\rho} = 1.2$ mm, PRE: $\hat{\rho} = 1.09$ mm, ANI-PRE: $\hat{\rho} = 1.1$ mm. Modelling the relevant portion of the tapered tip as a line with angle φ (figure 7), we can express the bone radius as $\xi(z) = \rho - \tan\varphi(z - z_A)$, where z_A marks the beginning of the tapered portion. We used the value $\varphi = \pi/4$ in all simulations. A longitudinal reaction force exists in the region $[z_A, z_B]$, where $z_B = z_A + (\rho - \hat{\rho})/\tan\varphi$ is the point at which $\xi = \hat{\rho}$. The pressure in this region is well approximated by the function

$$P(z) = \frac{P_0(1 - (z - z_A))}{z_B - z_A}. \tag{4.1}$$

From this, we obtain the axial component of the reaction force density

$$F_z(z) = -2\pi\xi(z)\sin\varphi P(z)\chi(z), \tag{4.2}$$

expressed as a force per axial length, where χ is a characteristic function for the region $[z_A, z_B]$.

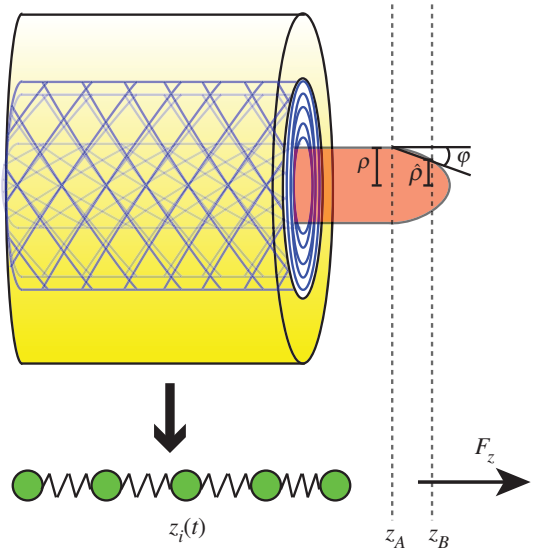

Figure 7. Schematic of model for tongue projection dynamics. The cylindrical tongue complex is mapped to a series of one-dimensional springs subject to a axial reaction force in the tapered region of the bone. (Online version in colour.)

Once the effective force $F_z(z)$ and the effective spring constant K are known, the dynamics of the system is simply governed by Newton's second law. Letting $z_i(t)$ denote the position of the ith point, $i = 1, 2, \ldots N$, we integrate forward the coupled system of equations

$$m_i \ddot{z}_i + \gamma \dot{z}_i + K\left(\frac{2z_i - z_{i+1} - z_{i-1}}{l} - 1\right) = F_z(z_i)l, \tag{4.3}$$

with appropriate one-sided spring forces at the endpoints $i = 1$ and $i = N$. Here, $m_i = m/N$ with m the total mass, $l = \tilde{l}/(N-1)$ the 'rest length' of each spring unit and γ is a damping coefficient. Once the tongue complex has completely left the bone, it has acquired its final velocity and simply extends telescopically until its tip reaches the prey. Our primary point of interest is to determine that velocity. Because the relevant dynamics occurs while the tongue is sliding off the bone, we do not explicitly model the telescoping process, and we consider the tongue complex as a single unit while on the bone (i.e. z_i denotes the position of the ith point of the entire tongue complex).

The simulated motions for the four cases of figure 5 are presented in figure 8. In each case, we have assumed that launch occurs at $v = 0.75$ such that the anterior 2 mm extends into the tapered region at time $t = 0$. For comparison, we reproduce the tongue motion as measured in *Trioceros melleri* [3]. For the solid lines in figure 8, the launch is simulated without drag. As expected, there is a correlation between the amount of internal energy and the maximum velocity. However, this relationship is highly nonlinear owing to the complex launching process. For instance, there is 56 mJ of stored energy in BASE, which would predict a maximum velocity of $10.5\,\mathrm{m\,s^{-1}}$ if all the energy were converted into directed axial motion, yet only $9.1\,\mathrm{m\,s^{-1}}$ is attained, even in a frictionless system. Also, while in ANI–PRE there is more than five times the amount of stored energy compared with ANI, the maximum velocity is less than double the amount. Such discrepancies between potential energy and realized axial kinetic energy reflect the fact that the full three-dimensional tissue will dynamically deform both radially and axially, so not all energy will contribute to directed axial motion.

For the dashed lines in figure 8, we take into account the effect of damping while on the bone, with damping coefficient γ proportional to the radial pressure, for BASE and ANI-PRE. Even with mild damping ($\gamma = 0.025 l P_0$), the maximum velocity is significantly decreased. With damping, BASE is slowed to $6.1\,\mathrm{m\,s^{-1}}$, similar to the typical measured peak velocity seen across a number of

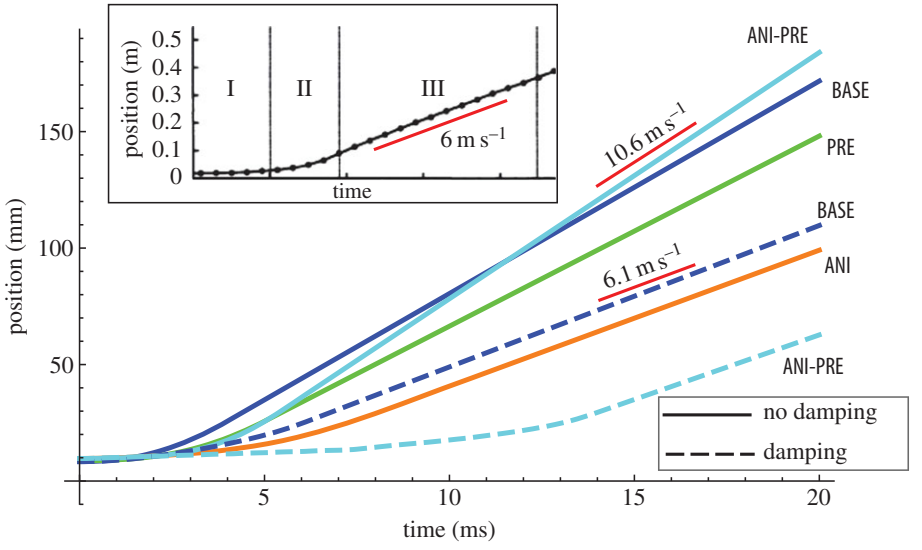

Figure 8. Mean position against time; inset shows measured data from *Trioceros melleri* from [3]. Solid lines simulate dynamics without damping, dashed lines include a damping term proportional to radial pressure. (Online version in colour.)

species [1,3,13]. Interestingly, the increased damping in ANI–PRE owing to the higher radial pressure negates the energy advantage of the residually stressed sheaths, so that the tongue complex for BASE departs the bone more quickly and with higher maximum velocity.

5. Discussion

In this paper, we have developed a mathematical framework for the firing mechanism of the chameleon tongue. Our results, while not an exhaustive analysis of the potential configurations, nevertheless, highlight the nonlinear dependence of measurable quantities on model parameters in this intriguing mechanical system. A natural question to ask is whether the system is optimized in some sense. From a biological standpoint, optimization is an appealing but difficult concept, strongly dependent on evolutionary history and specific situations. However, from a mechanical design perspective, it is perfectly reasonable to consider whether the mechanism elucidated here can be optimized in any particular, well-defined, sense by varying the geometrical configuration. One natural measure to consider in this regard is the maximum speed attained in the ballistic firing.

In figure 9, we examine the effect of two key control parameters on maximum speed: the fibre angle ϕ in the sheaths and the reference radius of the innermost sheath, A_1. In figure 9*a*, we plot the maximum speed and stored energy for varying ϕ and with all other parameters at the base values. In each case, we simulate the dynamics at $\nu = 0.75$ and with damping while on the bone proportional to radial pressure as above ($\gamma = 0.025lP_0$). At small fibre angles, there is not enough stored energy to overcome the damping and the tongue does not fire. At about 37°, a first-order transition is observed, and the maximum speed then increases monotonically as the fibres become more aligned with the axial direction. However, while axially oriented fibres produce the greatest speed, such a choice is deficient in other regards. As ϕ increases, the axial stiffness of the sheaths increases sharply. The effect of this is twofold: first, almost no axial extension is attained, a significant hindrance in reaching the tapered tip to fire. Second, high axial stiffness of the underlying layers is antagonistic to the muscle, which attempts to extend the complex axially when contracting. Hence, in order to achieve 30% contraction, the work requirements of the muscle rise significantly, with almost all energy stored in the muscle as $\phi \to 90°$. The angle

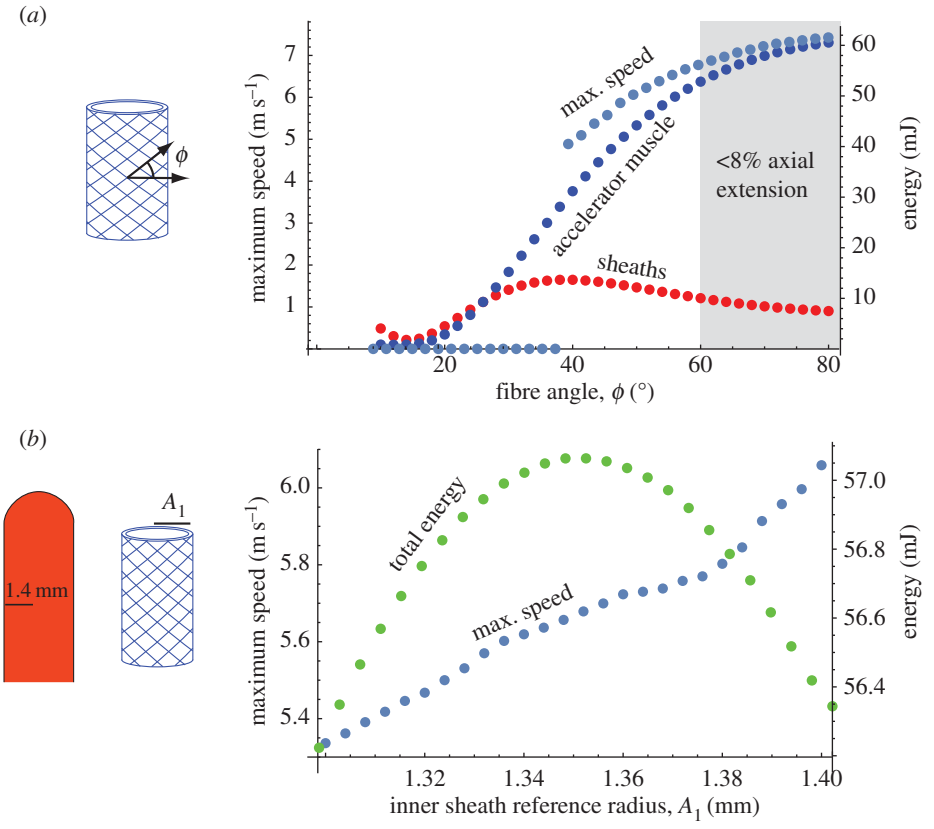

Figure 9. Maximum speed and stored energy with varying control parameters: (*a*) fibre angle in sheaths and (*b*) innermost sheath reference radius. (Online version in colour.)

range 40–60° provides a balance between speed, extension and energy storage, as it allows for significant axial extension while sheaths and muscle store similar amounts of energy.

In figure 9*b*, we repeat the analysis with varying inner sheath radius A_1. Here, any value less than 1.4 mm induces residual stress in the rest position. In all cases, with ϕ fixed at 50°, the axial stretch is greater than 10% and so we focus on the maximum speed. We plot in figure 9*b* both the total stored elastic energy and the maximum speed. The key feature is that even though the total stored energy achieves a maximum with non-zero residual stress ($A_1 \approx 1.35$), the maximum speed is monotonic, achieving a maximal value at the limiting case of no residual stress (note that A_1 cannot be taken beyond 1.4 mm, as the sheaths would be disconnected from the bone in the rest position). This computation demonstrates again the non-trivial relation between energy storage and energy release. With added residual stress, the pressure on the bone is higher, which creates a greater longitudinal reaction force; however, increased pressure also creates increased damping, ultimately resulting here in decreased speed. Hence, maximal potential elastic energy does not necessarily translate into maximal kinetic energy, which challenges the traditional view of biomechanics that high energy storage is the principal design goal.

While the results above demonstrate a potentially significant variation in firing velocity with material parameters, owing to the mechanical complexity of the firing mechanism, it has been observed that peak velocity is relatively constant across different species of chameleons [1,13]. This invariance is particularly intriguing when considering the relatively significant distribution in size found in chameleons, with body length (typically measured from snout to vent) varying by more than a factor of two between species. The size independence of velocity is attributed

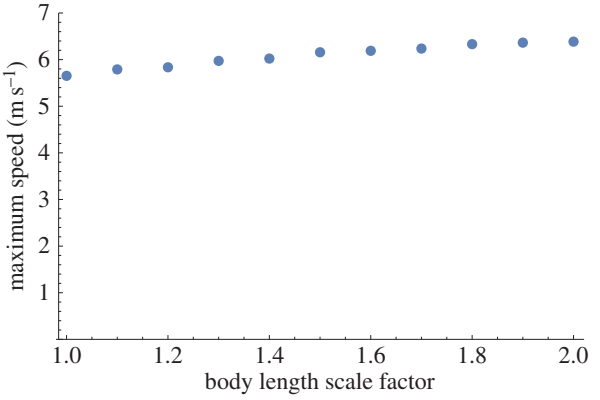

Figure 10. Maximum speed as a function of body scale factor α. When the body length doubles, the overall maximal velocity remains mostly constant. (Online version in colour.)

to the fact that smaller chameleons have proportionally larger tongue apparatuses—for instance, the tongue mass does not scale with the cube of the length of the chameleon's body, but rather is closer to the square of the length [13]. While a detailed analysis of interspecific variation and scaling of the tongue mechanism is beyond the scope of this study, it is worthwhile to comment on the effect of scale. In figure 10, we plot the maximum velocity as a function of body length scale factor α, i.e. the proportional increase in snout–vent body length from the base model parameters, which correspond to *T. jacksonii*. Thus, the left-most point $\alpha = 1$ corresponds to the base values, whereas the right-most point $\alpha = 2$ corresponds to a chameleon of double the length. For each value of α, we have scaled the tongue length l (scales as $\approx 0.8\alpha$), mass m (scales as $\approx \alpha^2$), bone radius ρ (scales as $\approx 0.8\alpha$) and accelerator muscle area (scales as $\approx \alpha/0.8$) according to the scaling laws in [13]. As seen in figure 10, the model correctly predicts a nearly constant peak velocity, with a variation of only about 10% across a 200% variation in body length.

The ballistic mechanism of the chameleon is a striking example of mechanical innovation and the use of elasticity to generate rapid motion in the animal kingdom. The analysis presented suggests that this mechanism involves a complex interplay between geometry (through the internal organization of intralingual sheaths and accelerator muscles), material properties (defined by the orientation of the collagen fibres, the pre-stress and the muscle activation) and mechanics (contraction–extension followed by expulsion). We have given a quantitative confirmation for the hypothesis that the ballistic mechanism requires energy storage in the collagenous intralingual sheaths coupled with muscular activity. Our model connects within a single mathematical framework the several distinct features necessary for successful projection: it requires sufficient initial tongue extension, internal elastic energy formed through the deformations and interactions of different layers, and a means of efficient energy conversion to produce directed motion.

Authors' contributions. D.E.M. and A.G. designed the research and co-wrote the paper. All authors contributed to the mathematical analysis.

Data accessibility. Calculations were performed using MATHEMATICA.

Competing interests. We have no competing interests.

Funding. We received no funding for this study.

References

1. Anderson CV. 2016 Off like a shot: scaling of ballistic tongue projection reveals extremely high performance in small chameleons. *Sci. Rep.* **6**, 18625. (doi:10.1038/srep18625)
2. Wainwright PC, Kraklau DM, Bennett AF. 1991 Kinematics of tongue projection in Chamaeleo-oustaleti. *J. Exp. Biol.* **159**, 109–133.

3. de Groot JH, van Leeuwen JL. 2004 Evidence for an elastic projection mechanism in the chameleon tongue. *Proc. R. Soc. Lond. B* **271**, 761–770. (doi:10.1098/rspb.2003.2637)
4. Müller UK, Kranenbarg S. 2004 Power at the tip of the tongue. *Science* **304**, 217–218. (doi:10.1126/science.1097894)
5. Wainwright PC, Bennett AF. 1992 The mechanism of tongue projection in chameleons. II. Role of shape change in a muscular hydrostat. *J. Exp. Biol.* **168**, 23–40.
6. Anderson CV, Deban SM. 2010 Ballistic tongue projection in chameleons maintains high performance at low temperature. *Proc. Natl Acad. Sci. USA* **107**, 5495–5499. (doi:10.1073/pnas.0910778107)
7. Roberts TJ, Azizi E. 2011 Flexible mechanisms: the diverse roles of biological springs in vertebrate movement. *J. Exp. Biol.* **214**, 353–361. (doi:10.1242/jeb.038588)
8. Higham TE, Anderson CV. 2013 Function and adaptation in chameleons. In *The biology of chameleons* (eds KA Tolley, A Herrel), pp. 63–83. Oakland, CA: University of California Press.
9. Houston J. 1828 On the structure and mechanism of the tongue of the chameleon. *Trans. R. Irish Acad.* **15**, 177–201.
10. Duvernoy G. 1836 Sur les mouvements de la langue du caméléon. *CR hebd. Séanc. Acad. Sci. Paris* **2**, 349–351.
11. Müller UK, Kranenbarg S. 2004 Power at the tip of the tongue. *Science* **304**, 217–219. (doi:10.1126/science.1097894)
12. Herrel A, Meyers JJ, Aerts P, Nishikawa KC. 2000 The mechanics of prey prehension in chameleons. *J. Exp. Biol.* **203**, 3255–3263.
13. Anderson CV, Sheridan T, Deban SM. 2012 Scaling of the ballistic tongue apparatus in chameleons. *J. Morphol.* **273**, 1214–1226. (doi:10.1002/jmor.20053)
14. Van Leeuwen JL. 1997 Why the chameleon has spiral-shaped muscle fibres in its tongue. *Phil. Trans. R. Soc. Lond. B* **352**, 573–589. (doi:10.1098/rstb.1997.0039)
15. Debray A. 2011 Manipulators inspired by the tongue of the chameleon. *Bioinspir. Biomim.* **6**, 1–15. (doi:10.1088/1748-3182/6/2/026002)
16. Deban SM, O'Reilly JC, Dicke U, Van Leeuwen JL. 2007 Extremely high-power tongue projection in plethodontid salamanders. *J. Exp. Biol.* **210**, 655–667. (doi:10.1242/jeb.02664)
17. Deban SM, Richardson JC. 2011 Cold-blooded snipers: thermal independence of ballistic tongue projection in the salamander *Hydromantes platycephalus*. *J. Exp. Zool. A, Comp. Exp. Biol.* **315A**, 618–630. (doi:10.1002/jez.708)
18. Kier W, Smith K. 1985 Tongues, tentacles and trunks: the biomechanics of movement in muscular-hydrostats. *Zool. J. Linn. Soc.* **83**, 307–324. (doi:10.1111/j.1096-3642.1985.tb01178.x)
19. Vandiver R, Goriely A. 2008 Tissue tension and axial growth of cylindrical structures in plants and elastic tissues. *Europhys. Lett.* **84**, 58004. (doi:10.1209/0295-5075/84/58004)
20. Goriely A, Vandiver R. 2010 On the mechanical stability of growing arteries. *IMA J. Appl. Math.* **75**, 549–570. (doi:10.1093/imamat/hxq021)
21. Hofhuis H *et al*. In press. Morphomechanical innovation drives explosive seed dispersal. *Cell*.
22. van Leeuwen JL. 1997 Why the chameleon has spiral-shaped muscle fibres in its tongue. *Phil. Trans. R. Soc. B* **352**, 573–589. (doi:10.1098/rstb.1997.0039)
23. Van Leeuwen JL, De Groot JH, Kier WM. 2000 Evolutionary mechanics of protrusible tentacles and tongues. *Netherlands J. Zool.* **50**, 113–139. (doi:10.1163/156854200505900)
24. Herrel A, Meyers JJ, Nishikawa KC, De Vree F. 2001 Morphology and histochemistry of the hyolingual apparatus in chameleons. *J. Morphol.* **249**, 154–170. (doi:10.1002/jmor.1047)
25. Goriely A, Tabor M. 2013 Rotation, inversion and perversion in anisotropic elastic cylindrical tubes and membranes. *Proc. R. Soc. A* **469**, 20130011. (doi:10.1098/rspa.2013.0011)
26. Ogden RW. 1984 *Non-linear elastic deformation*. New York, NY: Dover.
27. Triantafyllidis N, Abeyaratne R. 1983 Instabilities of a finitely deformed fiber-reinforced elastic material. *J. Appl. Mech.* **50**, 149–156. (doi:10.1115/1.3166983)
28. Kassianidis F, Ogden R, Merodio J, Pence TJ. 2008 Azimuthal shear of a transversely isotropic elastic solid. *Math. Mech.Solids* **13**, 690–724. (doi:10.1177/1081286507079830)